



**HAL**  
open science

## Mechanical characterization and identification of material parameters of porcine aortic valve leaflets

Yannick Tillier, Colin Laville, Christophe Pradille

### ► To cite this version:

Yannick Tillier, Colin Laville, Christophe Pradille. Mechanical characterization and identification of material parameters of porcine aortic valve leaflets. *Journal of the mechanical behavior of biomedical materials*, 2020, 112, pp.104036. 10.1016/j.jmbbm.2020.104036 . hal-02986597

**HAL Id: hal-02986597**

**<https://minesparis-psl.hal.science/hal-02986597>**

Submitted on 5 Sep 2022

**HAL** is a multi-disciplinary open access archive for the deposit and dissemination of scientific research documents, whether they are published or not. The documents may come from teaching and research institutions in France or abroad, or from public or private research centers.

L'archive ouverte pluridisciplinaire **HAL**, est destinée au dépôt et à la diffusion de documents scientifiques de niveau recherche, publiés ou non, émanant des établissements d'enseignement et de recherche français ou étrangers, des laboratoires publics ou privés.



Distributed under a Creative Commons Attribution - NonCommercial 4.0 International License

# Mechanical Characterization and Identification of Material Parameters of Porcine Aortic Valve Leaflets

Colin Laville<sup>a</sup>, Christophe Pradille<sup>b</sup>, Yannick Tillier<sup>c1</sup>

<sup>a</sup> CEMEF Centre de Mise En Forme des Matériaux MINES ParisTech, PSL Research University  
CNRS UMR 7635 CS10 207  
06904 Sophia Antipolis Cedex  
France  
colin.laville@mines-paris.org

<sup>b</sup> Mat Xper Company  
19 traverse du barri  
sophia Antipolis  
06560 valbonne  
France  
christophe.pradille@mat-xper.com

<sup>c</sup> CEMEF Centre de Mise En Forme des Matériaux MINES ParisTech, PSL Research University  
CNRS UMR 7635 CS10 207  
06904 Sophia Antipolis Cedex  
France  
yannick.tillier@mines-paristech.fr

## ABSTRACT

*The ideal artificial heart valve does not exist yet. Understanding of mechanical and structural properties of natural tissues is necessary to improve the design of biomimetic aortic valve. Besides these properties are needed for the finite element modeling as input parameters. In this study we propose new method combining biaxial tests and digital image correlation. These tests are carried out on porcine aortic valves. In this work, we use a modified version of the HGO (Holzapfel-Gasser-Ogden) model which is classically used for hyper-elastic and anisotropic soft tissues. This model can include fiber orientation. The identification of HGO model parameters can be determined using experimental data and two different*

---

<sup>1</sup> Corresponding author

*protocols. One protocol is based on the identification of collagen fibers orientation as well as the mechanical parameters. The second one, is based on a complementary experiment to determine orientation (confocal laser scanning microscope). Both lead to determine different sets of material parameters. We show that the model is more likely to reproduce the actual mechanical behavior of the heart valves in the second case and that a minimum of three different loading conditions for the biaxial tensile tests is required to obtain a relevant set of parameters.*

## 1 INTRODUCTION

Aortic valves (AV) have the highest mortality rate among heart valve diseases (67,5% according to (Mozaffarian et al., 2016)). Treatment often consists of repairing the valve or replacing it with artificial valves. Although replacement of AV is one of the most common cardiovascular surgical procedures, its outcome is still difficult to predict, mainly due to the design and choice of materials used to manufacture the prostheses. Prosthetics manufactured by biomimetic engineering could be a promising alternative to current products. They could be indeed designed to allow natural hemodynamics, should not require anticoagulant treatment if they are treated to achieve better biocompatibility and be more durable (Ghanbari et al., 2009; Kidane et al., 2009). But their development requires prior and thorough characterizations of the mechanical behavior of natural valves. Developments can also greatly benefit from finite element modeling which requires well suited constitutive laws with the right sets of material parameters.

Heart valves are passive tissues that open and close under the influence of differential blood pressure (Sacks et al., 2009). AV leaflets are tri-layered structure composed of type I wavy collagen, elastin and glycosaminoglycans (GAGs) (Sacks et al., 2009). The top layer, called Fibrosa is the thickest layer (around 40% of the total thickness) and consists mainly of crimped and strongly oriented collagen fibers (50% by dry weight) and to a lesser extent elastin (10%) (Mohammadi and Mequanint, 2011). According to (Stella and Sacks, 2007) and (Buchanan and Sacks, 2014), it seems to be the main layer in terms of mechanical behavior. For this reason, we focus mainly on it in this

study. The bottom layer (around 30% of the total thickness), the ventricularis, is mainly composed of elastin and collagen fibers (Lee et al., 2001). It is highly elastic. It seems to help reduce large radial strains and help fibrosa to remain in a crimped configuration at rest (Vesely, 1998). The central layer of spongiosa has a high concentration of GAGs. They provide a damping mechanism to reduce the flutter leaflet when it is not subjected to a high tensile stress. The presence of collagen and elastin fibers gives the spongiosa a good delamination resistance thanks to interconnections with the adjacent layers (Eckert et al., 2013).

This work aims to demonstrate the feasibility of a new method:

- to measure the mechanical response of aortic valves
- to identify relevant material model parameters by means of biaxial testing, digital image correlation, and structural information obtained using a confocal laser scanning microscope coupled with an inverse analysis procedure.

Another objective of this study is to identify the nature and quantity of observables that must be considered in an inverse analysis procedure in order to obtain a set of parameters representative of the material. To simplify the process of supplying biological tissues, this study was carried out on porcine aortic valves but all steps described here can be easily applicable to human tissues. This entire procedure can also be implemented to ensure that the properties of future artificial valves match those of natural valves.

## **2 MATERIAL AND METHODS**

### **2.1 Experimental Study**

Because AV leaflets are thin (and almost incompressible), biaxial planar tests were chosen to quantitatively characterize their mechanical properties (Sacks and Sun, 2003). A similar approach was used to characterize the mechanical response of tricuspid (Amini Khoiy and Amini, 2016) and aortic (Billiar and Sacks, 2000) porcine valvular leaflets, but without 3D digital image correlation that is supposed to provide a more accurate description of strain fields. In order to obtain information on the local orientation of collagen fibers, samples in the fibrosa layer were observed by confocal laser scanning microscopy.

#### *2.1.1 Biaxial Tensile Testing Machine*

A custom biaxial tensile test device, designed and manufactured in our laboratory, was used in this study (Fig.1).

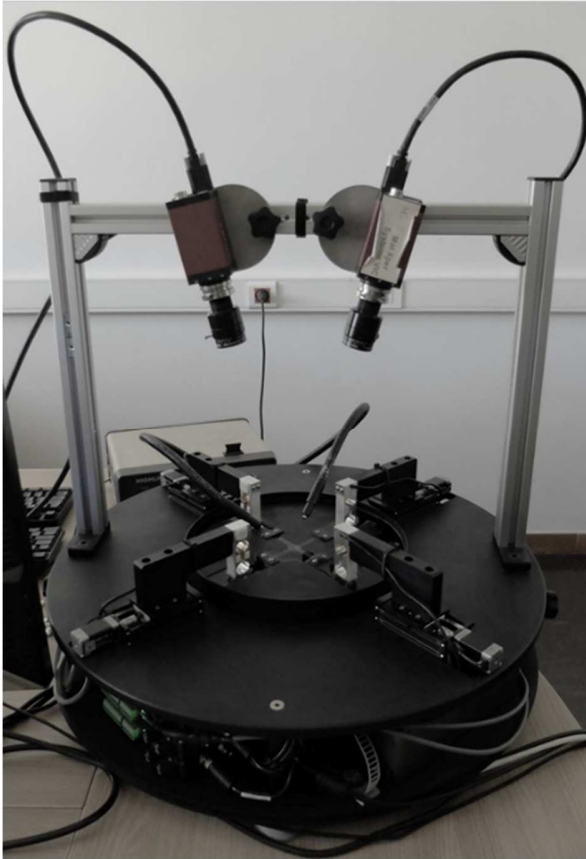


*Fig. 1: Custom biaxial tensile device*

It consists of four synchronized and motorized arms, allowing a maximum displacement of 25 mm each and a minimum step of 0.05  $\mu\text{m}$ . Speed ranges from 0.07  $\mu\text{m}\cdot\text{s}^{-1}$  and 26  $\text{mm}\cdot\text{s}^{-1}$ . Each arm is equipped with a 50 N load cell (sensitivity of 0.001 N). For biaxial tensile tests, three types of gripping mechanisms are commonly used in the literature: clamps, rakes, and sutures. While rake-based systems limit the amount of counter-lateral forces on the sample, they are much easier to mount repeatedly and evenly spaced. Rakes seem to result in a more uniform distribution of the load. Therefore, rake-based systems are often the method of choice when testing samples with symmetric material axes that can be aligned with the test axes (Fehervary et al., 2016).

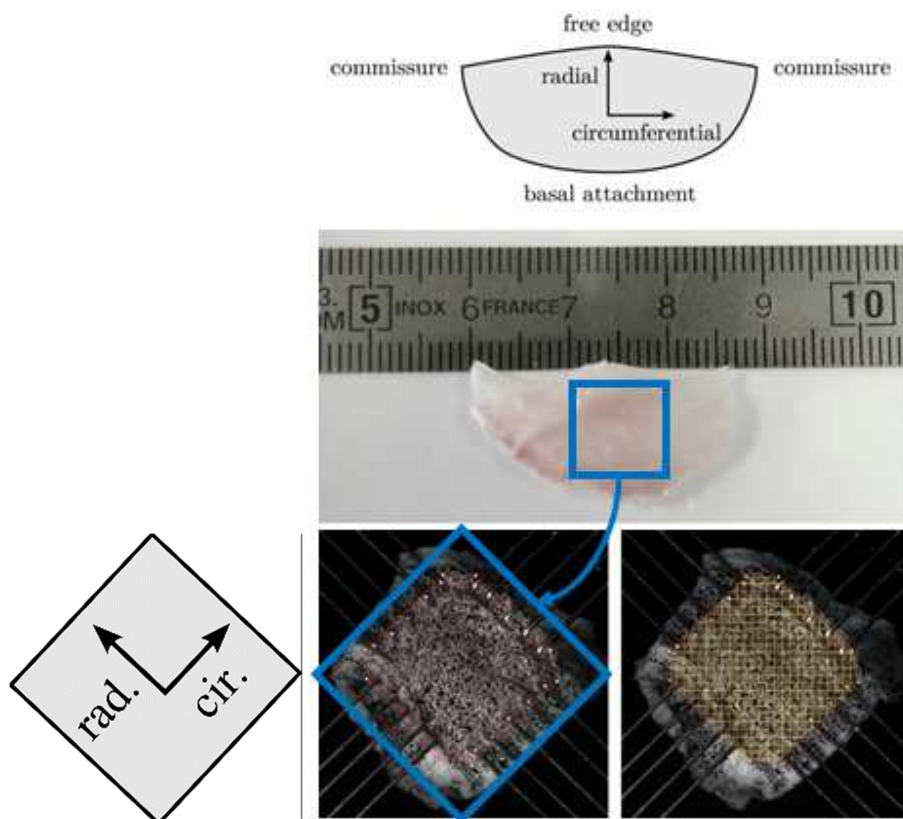


Fig. 2: Dissected porcine AV leaflet: square-shaped sample with gripping device and speckle pattern (subset grid size of 29 px)

In our case, specimens are gripped with five rake “teeth” (Fig. 2) on each side (with an initial spacing of 1 mm from each other). The minimum area between the hooks is  $7 \times 7 \text{ mm}^2$ . The arms are controlled while on the move thanks to a customized graphical user interface designed with NI LabVIEW® software.

2D imaging system is sensitive to out of plane motion (Sutton et al., 2008). In order to avoid this issue, two cameras are placed above the specimen to measure the displacement field thanks to a three-dimensional Digital Image Correlation (3D-DIC) system. It consists of AVT® PIKE cameras from Allied Vision Technologies GmbH with a resolution of 5 MP, with a maximum frame rate of 14 frames per second. 50-millimeter

Schneider Kreuznach photographic lens are mounted. Two coherent light sources are placed on the device to light up the surface of the sample constantly and uniformly.

### 2.1.2 Specimen Preparation

Two frozen and two fresh porcine hearts (about 5 months old, 80 kg) were obtained from a slaughterhouse. For fresh hearts, sample preparation and experiments were carried out on the day of delivery. The three leaflets of each AV were carefully dissected using a surgical scalpel, which means that a total of twelve samples were analyzed in this study. For each leaflet specimen, one square-shaped sample of about 10 mm on each side was taken from the central (lower belly) area (Fig. 2). In order to preserve their mechanical properties, the samples were stored and tested into 0.9% isotonic saline solution at room temperature during the experiment (less than 30 minutes). In order to capture local strain using DIC, a speckle pattern was applied to the surface of each sample, but their wet surface condition prevents a fast drying of the ink. After several attempts, the Black Bombay India Ink suggested by Genovese et al. (Genovese et al., 2011) was finally used since it is a fast-drying waterproof ink and it is also known that it doesn't alter the mechanical behavior of soft tissues. To facilitate application, the surface was quickly dried with a jet of compressed air at room temperature. Then, the ink was sprayed with a low-pressure airbrush (0.5 bar with a 0.5 mm pipe) until the speckle pattern uniformly covered the surface. The samples were then dried for less than 5 minutes in ambient air before being mounted on the biaxial device and immersed into isotonic saline solution. A foam holder was used to limit deformation and damage of the samples when inserting the rake teeth and then

removed before the test. The circumferential direction (the one from one commissure to the other, Fig. 2) was aligned as much as possible with one of the stretching directions.

### *2.1.3 DIC Protocol*

Before using the biaxial tensile testing device, the DIC system (Correlated Solution 's VIC-3D® system) was set up. Each camera was focused using the maximum aperture size. Then, the aperture opening was reduced to increase the depth of field during image recording. This is an important parameter to maintain focus in case of out-of-plane movements. The system was calibrated using a standard calibration grid. The accuracy of the entire procedure depends heavily on the quality of the calibration process, which ensures the dimensional consistency of the system.

For post-processing on the 3D-VIC® software, the subset size (Fig. 2) and the step (subset overlapping) were determined, according to the size, distribution and contrast of the speckle pattern. They are also optimized using the methodology described in (Candau et al., 2016), to ensure effective analysis of the displacement fields within an acceptable time. Three virtual extensometers were placed and averaged on each axis to measure the actual displacement of the sample boundaries. The average of the strain was calculated in the central area of the samples.

### *2.1.4 Biaxial Tensile Testing Protocol*

A small preload of 0.01 N was first applied to slightly stretch the samples. From this loading state, the specimens were preconditioned using three continuous loading/unloading cycles. Preconditioning cycles were equibiaxial (1:1) in force with a

threshold value of 0.5 N and carried out at a constant speed of 0.01 mm.s<sup>-1</sup>. The samples were subjected to seven successive loading conditions ( $T_x:T_y$ )={ (1:1), (1:0.5), (1:0.25), (1:0.1), (0.25:1), (0.5:1), (1:1)}, where ( $T_x:T_y$ ) represents the force threshold ratio on each axis (respectively x and y) depending on the loading protocol. Thus, each axis stops independently when it reaches its own force threshold. The maximum value of 1 is reached when the force is equal to 0.5 N. This value was chosen to correspond to the in vivo membrane tension peak of 60–80 N.m<sup>-1</sup> which occurs during diastole (Sacks et al., 2009). Since the tissues of the AV leaflet do not exhibit time-dependent effects under physiological loading conditions (Stella et al., 2007), a single displacement velocity at 0.01 mm.s<sup>-1</sup> was prescribed for all experiments. Each protocol (from excision to the end of the last loading/unloading cycle) lasted less than two hours. To ensure that the tissue was stabilized after preconditioning and was not damaged during the experiments, the last (1:1) loading was systematically compared to the first. Once the experiments were completed, five thickness measurements were taken at different locations using a digital micrometer (with a resolution of 2 μm) and the average was calculated. Measurements were not performed before the experiments to avoid any damage to the samples.

#### 2.1.5 Confocal Laser Scanning Microscopy Protocol

In order to avoid any deterioration of the collagen fibers due to cryopreservation as shown for instance in (Schenke-Layland, 2008), only two fresh samples were observed under a confocal laser scanning microscope. The observations focus on the collagen fibers in the fibrosa layer, which is the main layer with regard to mechanical behavior. The first sample was a square collected in the central region (lower belly) of a

leaflet previously tested on the biaxial tensile machine. The second sample was a whole leaflet that did not undergo any ex vivo mechanical loading. The experiments were performed on a Leica TCS SP2 SE confocal microscope. A x40 water immersion objective (Fig. 3) was mounted on the microscope and the zoom was set to x1.7.

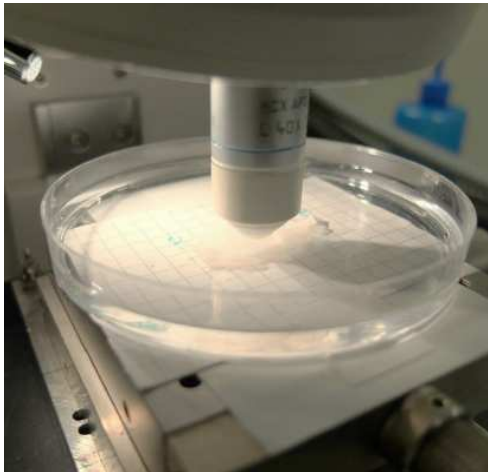


*Fig. 3: Specimen examined under the confocal laser scanning microscope*

The resulting images were 12-bit images with a total size of  $220 \times 220 \mu\text{m}^2$  and a resolution of  $1024 \times 1024$  pixels. The surface of the samples was carefully dried with a fabric to glue them in a Petri dish, in their undeformed state, with a cyanoacrylate adhesive. The glue was applied on the ventricularis side to observe the fibrosa layer. The petri dish was filled with 0.9% isotonic saline solution and fixed to the microscope stage. To excite collagen fibers in all directions, a laser beam of circularly polarized light at 830 nm (COHERENT® Chameleon Vision) was used. A reference point was taken on a grid under the Petri dish. From this point on, a series of stacks of 2D images were taken knowing the plane coordinates of each measurement. A surface area of  $5 \times 5 \text{mm}^2$  located in the center of the sample was scanned. Thanks to a micrometric xy displacement stage, image acquisitions were made every millimeter in the

circumferential direction and every half millimeter in the radial direction. Due to the specific structure of the collagen fibers in the fibrosa layer (3.4), the automated identification of local fiber orientations presents many practical difficulties. The quasi-continuous structure of uniformly crimped fibers makes it very difficult to use a segmentation algorithm to identify preferred fibers orientations. The local orientation was therefore measured manually using the ImageJ software (Ferreira and Rasband, 2012). For each image, a single local main fiber direction was obtained by averaging ten angle measurements. The local average angles were then interpolated on a fine regular grid by means of a Python script that used cubic spline functions.

## **2.2 Numerical Study**

An inverse analysis procedure was performed to select and calibrate a material model. It is based on the comparison between the biaxial experiments (introduced in section 2.1.4) and a finite element model used to numerically reproduce these experiments.

### *2.2.1 Constitutive Equations*

Numerical developments have been carried out as part of the FORGE® NXT (TRANSVALOR S.A) commercial finite element software developed in our laboratory. AV leaflets are idealized as a homogeneous and incompressible material. An anisotropic and hyperelastic constitutive model was implemented using an updated Lagrangian method in the finite strain framework. A modified version of the transversely isotropic Holzapfel-Gasser-Ogden (HGO) model, first introduced in (Holzapfel et al., 2000) for the

description of the mechanical response of arterial tissues, was chosen. The isochoric contribution of the strain-energy function  $W$  is:

$$W = \frac{c_0}{c_1} [e^{c_1(\bar{I}_1-3)} - 1] + \frac{c_2}{2c_3} [e^{c_3(\kappa\bar{I}_1+(1-3\kappa)\bar{I}_4-1)^2} - 1] \quad (1)$$

where  $c_0, c_1$  and  $c_3$  are positive material parameters and  $\kappa \in [0, \frac{1}{3}]$  is the fiber structure dispersion parameter as defined in (Gasser et al., 2006). In the case of transversely isotropic,  $\kappa$  is obtained as follows:

$$\kappa = \frac{1}{4} \int_0^\pi \rho(\theta) \sin^3(\theta) d\theta \quad (2)$$

where  $\theta$  corresponds to the fiber orientation angles (those measured using confocal laser scanning microscopy in our case),  $\rho(\theta)$  is the normalized  $\pi$ -periodic von Mises distribution centered on  $\theta = 0$ . As suggested by Wang et al. (Wang et al., 2014) for the modeling of the human left ventricle in diastole, the potential of the non-collagenous neo-Hookean matrix of the HGO model  $c_0(\bar{I}_1 - 3)$  (Holzapfel et al., 2000) is replaced by a Fung-type exponential strain-energy function  $\frac{c_0}{c_1} [e^{c_1(\bar{I}_1-3)} - 1]$  to better capture the non-linear behavior of the groundmatrix.

This model is able to consider some structural information, such as a local statistical distribution of fibers. Assuming that local orientations for the principal fibers can be correlated to the macroscopic directions of the anisotropy, an algorithm was developed to transpose the orientations identified by confocal microscopy (2.1.5) into the finite element model. It allows to define an initial direction of anisotropy and a dispersion parameter on each element. Due to the very locally aligned structure of the collagen fibers (3.4), the dispersion parameter was set to 0, which allowed to consider a

material homogenized with the orientations of the collagen fibers of the fibrosa layer. The stability and accuracy of the numerical implementation has been verified through several numerical tests (volume conservation accuracy, mechanical response, energy conservation).

### 2.2.2 Inverse Analysis Protocol

An inverse analysis procedure was carried out to calibrate the modified HGO material model. A kriging metamodel-assisted evolutionary algorithm was used (Roux, 2011; Roux and Bouchard, 2013, 2015). A biaxial tensile test was numerically reproduced with a simplified 5 x 5 mm<sup>2</sup> geometry corresponding to the area between the rakes. It consists in a 0.25 mm structured mesh, with a total of 3600 linear tetrahedral elements. A minimum of 2 elements in the thickness has been respected in order to limit an artificial stiffening of the structure. A homogeneous thickness of 0.5 mm was used (3.1).

The displacements measured with the digital image correlation system were imposed as boundary conditions and the inverse analysis procedure was performed on the measured force on each axis.

For the *i*-th loading condition, the objective function to minimize is defined as a least squares function following the equation:

$$f_i(x) = \sqrt{\frac{\sum_{j=1}^m (F_j^{exp}(x) - F_j^{num}(x))^2}{\sum_{j=1}^m (F_j^{exp}(x))^2}} \quad (3)$$

We denote the number of experimental points,  $F_j^{exp}$  the experimental force values and  $F_j^{num}$  the corresponding (interpolated) force values given by the numerical model.

Since several observable variables (different loading conditions) were used at each evaluation step of the inverse analysis procedure, an average objective function  $\bar{f}(x)$  was used, defined as follows

$$\bar{f}(x) = \frac{1}{obs} \sum_{i=1}^{obs} f_i(x) \quad (4)$$

where *obs* is the number of observable variables.

### 3 RESULTS

#### 3.1 Thickness Measurements and Damage Follow-Up During the Test

The thickness of the different valves is globally constant (Fig. 4), with an average value of 0.525 mm, although the measurement can vary from one leaflet to another, with a variation from 45 to 97  $\mu\text{m}$  around the average value.

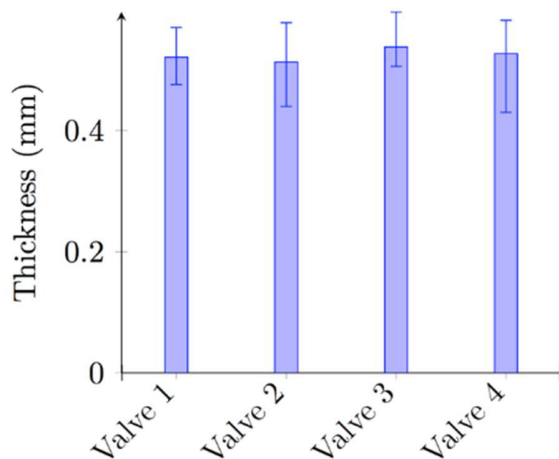


Fig. 4: Averaged thickness of the samples with dispersion for each valve (Valves 1 & 2 are frozen; valves 3 & 4 are fresh)

In Fig. 5, it can be seen that the first and the last (1:1) loadings are superimposed. This was systematically the case, confirming that three preconditioning cycles are effective enough and that no damage occurs during the different tests.

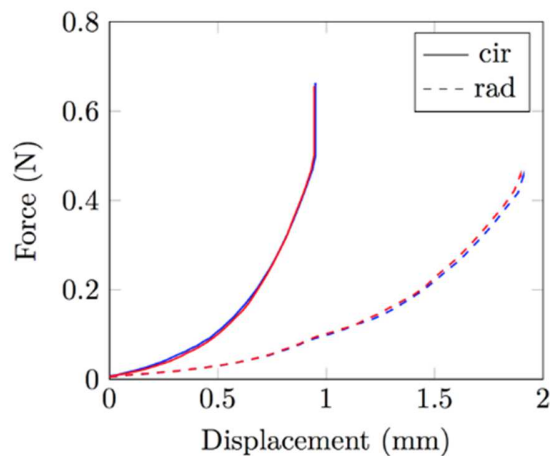


Fig. 5: (1:1) curves obtained at the beginning and at the end of a full loading protocol, on the same sample

### 3.2 3D-DIC Strain Fields

Examples of 3D-DIC strain field measurements (when the maximum load is reached) on a sample are shown in Fig. 6. The strain in the radial and circumferential directions corresponds to  $\varepsilon_{xx}$  and  $\varepsilon_{yy}$  respectively. The definition of nominal strain is used because the strain levels are low. On frozen and fresh samples, and for all types of loading, the results show very heterogeneous strain fields, in both directions. The loading is probably not purely biaxial in some areas, due to an imperfect but inevitable alignment of the rakes. Local strain concentrations can indeed be observed near the rakes and at the corners of the samples. They do not strongly affect the central area of the samples (almost the central quarter of the specimen). According to the literature (Avril and Evans, 2017; Sacks and Sun, 2003), these results clearly demonstrate the

anisotropic behavior of the tissues, with the circumferential direction being stiffer than the radial direction.

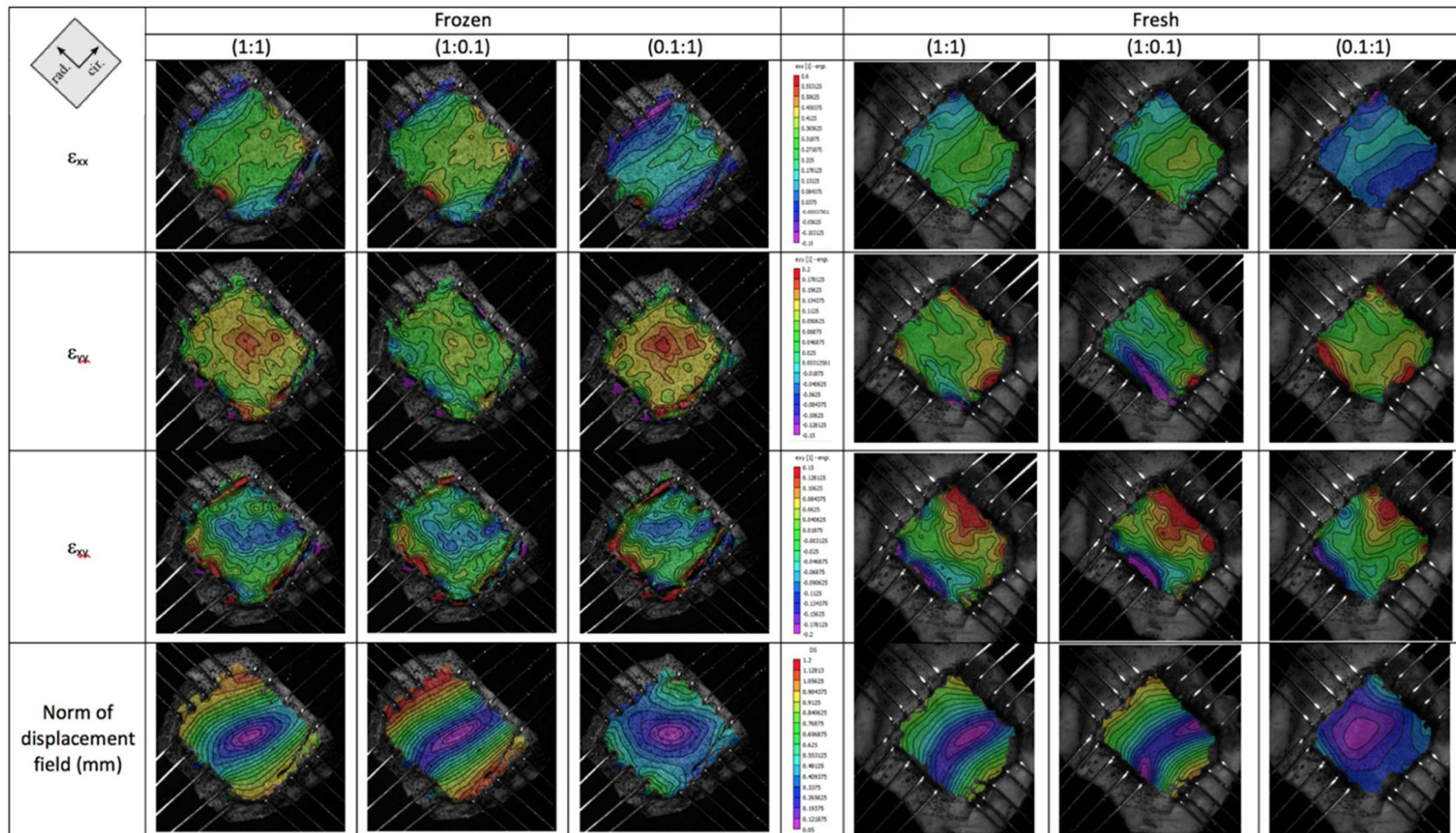
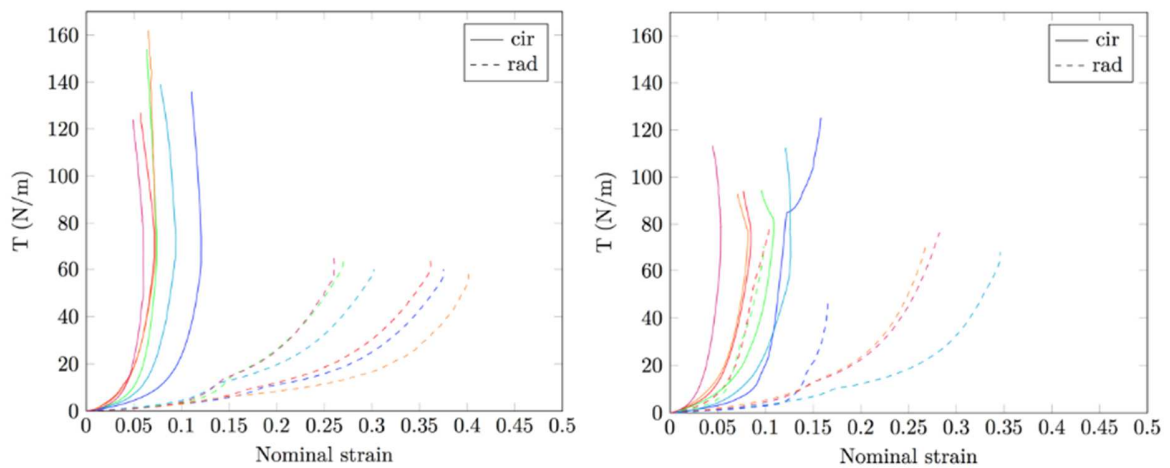


Fig. 6: Strain and norm of displacement fields obtained on frozen (left) and fresh (right) samples

### 3.3 Tension-Strain Results

The average strain in each direction was calculated in a circular area in the center of the samples, in areas where rakes have no effects, as indicated in the previous subsection. The average strain increases with the selected surface area, moving increasingly closer to the rakes. However, in the 25% central region, the effect of the surface area on measurements remains small.

As has been done in similar studies (Amini Khoiy and Amini, 2016; Sacks, 2000), we subsequently used the membrane stress (or tension) in N/m. Fig. 7 shows an example of tension-strain results for several frozen and fresh samples.



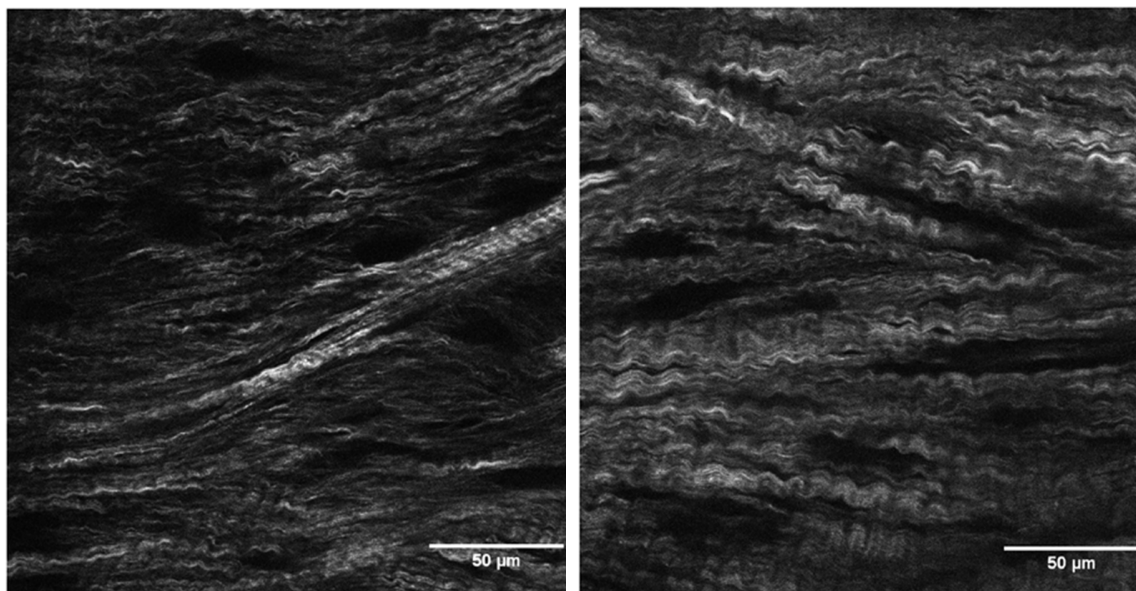
*Fig. 7: Example of tension-strain curves for the (1:1) loading condition for several frozen (left) and fresh (right) samples*

A significant dispersion of the curves in both radial and circumferential directions can be observed. In addition, fresh samples show significant differences in their mechanical response compared to frozen samples, such as lower levels of strain and stress and stronger coupling between the stretch axes. While the experimental results show some scattering of the mechanical response between samples, both for fresh and frozen conditions, there is no significant difference between the leaflets belonging to

the same valve. A highly non-linear mechanical behavior can be observed. Tissues are much more compliant in the radial direction than in the circumferential direction, resulting in large disparities in stretchability. The stress and strain levels are significantly lower for fresh tissues, as well as the non-linearity of the stress-strain curves. Turning points appear on some curves, due to the fact that the motors stop on one axis but the biaxial test machine continues to pull the sample on the other one. A strong coupling can be observed between the axes.

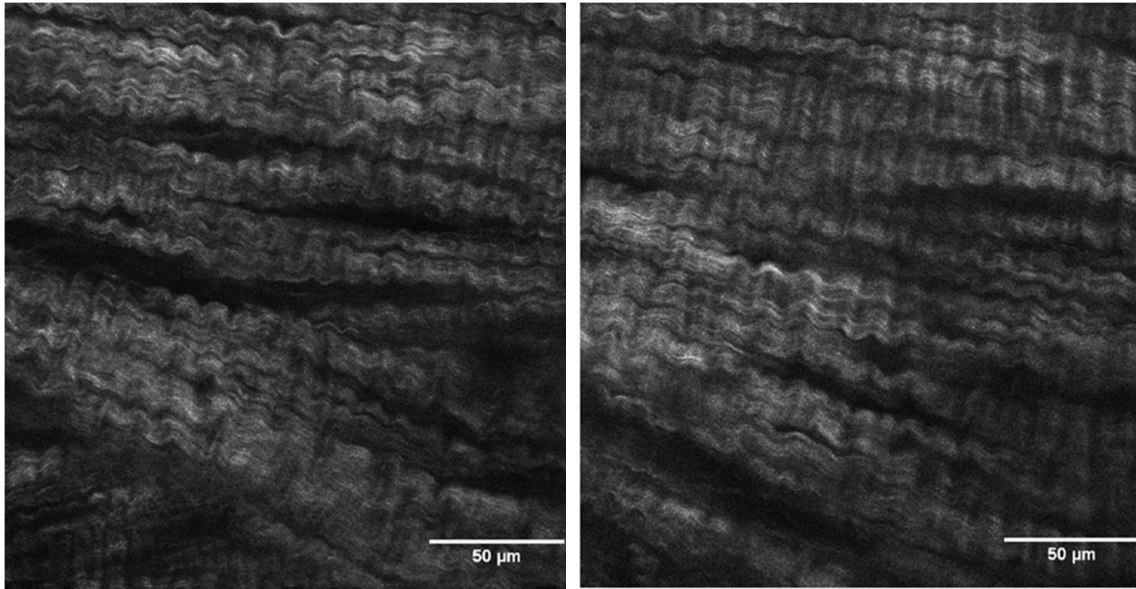
### 3.4 Confocal laser scanning microscopy results

The results of confocal microscopy showed that the orientation of collagen fibers changes considerably with depth in the first 100  $\mu\text{m}$  from the surface. From a randomly oriented state near the surface, the collagen fibers move to a very aligned state in the fibrosa layer. An example of images from a stack with a depth of 140  $\mu\text{m}$  is shown on Fig. 8.



a) 50  $\mu\text{m}$  depth

b) 80  $\mu\text{m}$  depth



c) 110  $\mu\text{m}$  depth

d) 140  $\mu\text{m}$  depth

*Fig. 8: Four pictures of collagen fibers from a total stack of 140  $\mu\text{m}$  depth*

Once the fibrosa layer is reached, the scattering of local collagen fibers orientation drastically reduces with small orientation changes between 110 and 140  $\mu\text{m}$  depth. Moreover, the fibers are mainly oriented in the focal plane. Fig. 9 shows an example of the results for the mechanically tested sample.

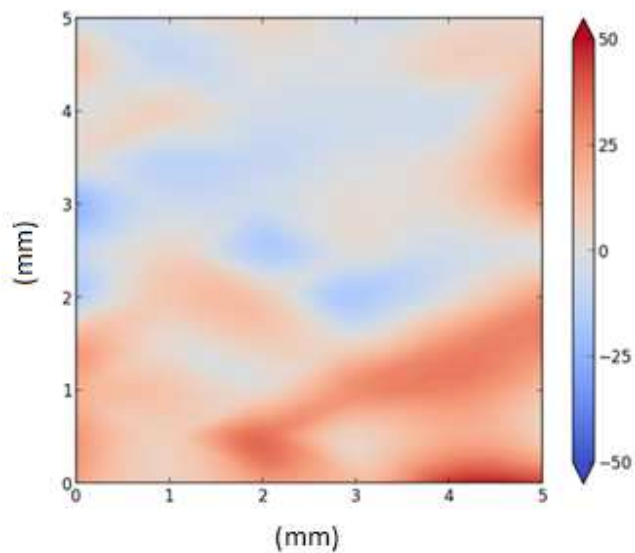


*Fig. 9: Interpolated angles ( $^{\circ}$ ) on a real scale grid (mm) for the mechanically tested sample*

The preferred fiber directions are mainly oriented in the circumferential direction  $0 \pm 10^\circ$ . However, regional disparities can be observed with maximum angles of about  $\pm 50^\circ$ .

### 3.5 Inverse analysis results

In order to assess the influence on the results of the number of different loading conditions to be considered, several inverse analysis procedures were carried out, applying the displacements measured from DIC. **The numerical setup used reproduces the biaxial experiment on the  $5 \times 5 \text{ mm}^2$  area between the rakes. Fiber orientation and dispersion parameters previously obtained from confocal measurements were transposed to the finite element mesh using a homemade algorithm in order to approximate the fibrous structure of the sample (Fig. 10).**

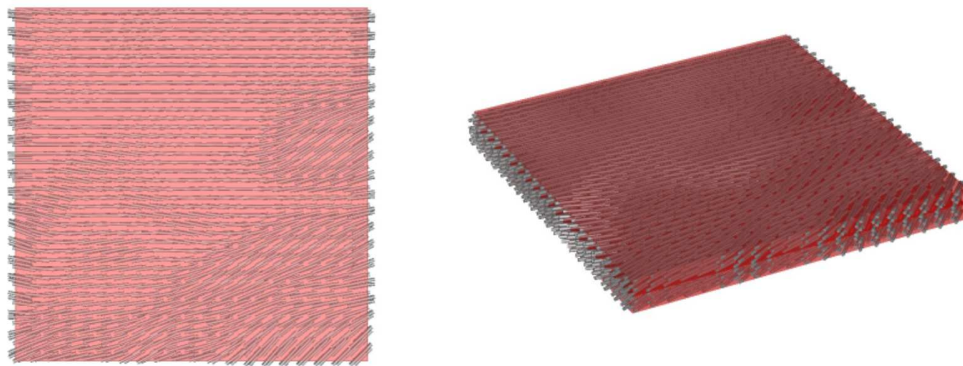


*Fig. 10: Interpolation of measured fibers directions on the undeformed finite element mesh*

A comparison of the experimentally and numerically obtained curves with the best set of parameters is presented in Fig. 11.

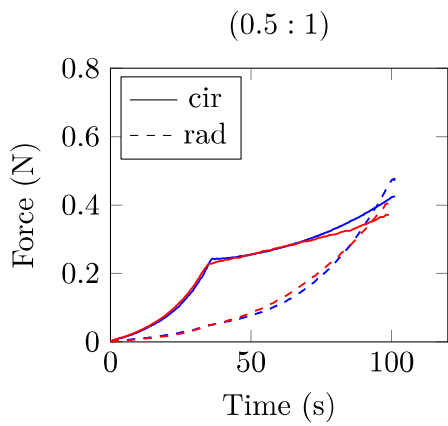
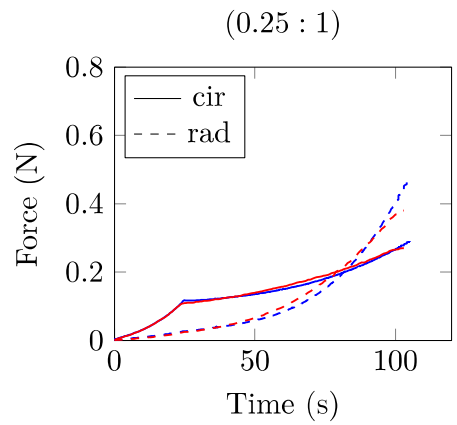
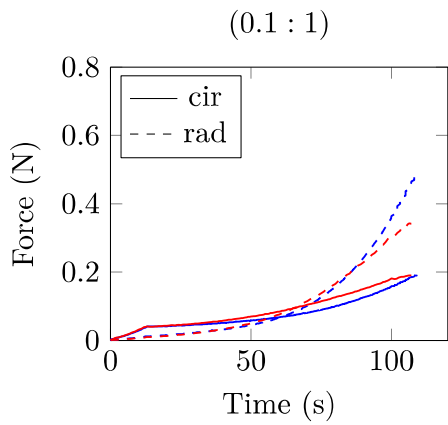
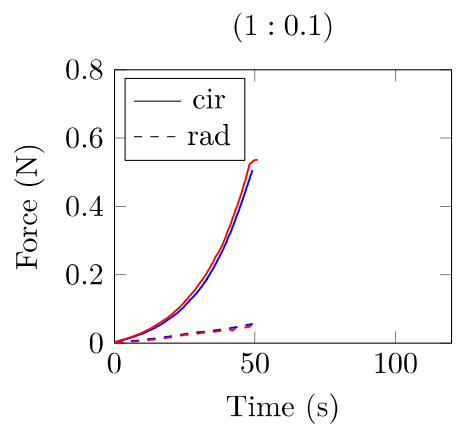
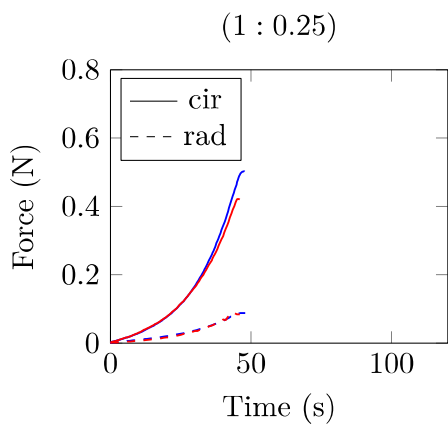
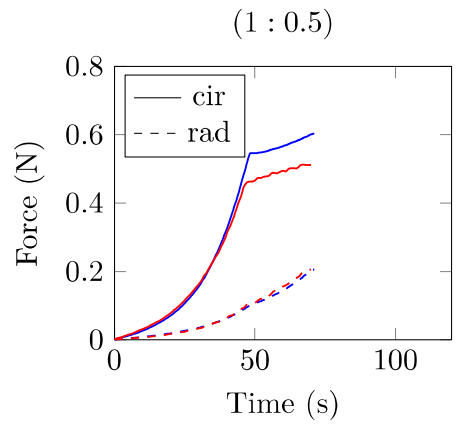
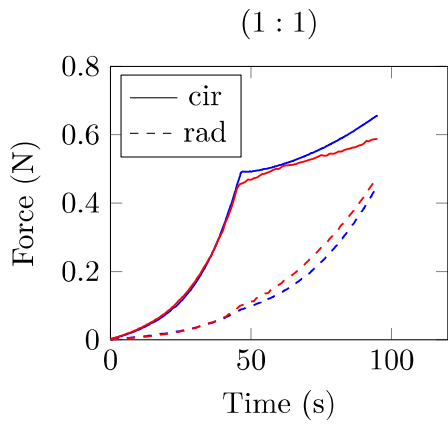


*Fig. 11: Forces in radial and circumferential directions from experimental (blue) and inverse analysis (red) results. Local fiber orientation, measured with confocal microscopy, was fixed and interpolated on each element*

These results were obtained by defining a local anisotropy direction from confocal images on each element. Another attempt was made on curves with seven loading conditions, letting free a global homogeneous fiber orientation angle in the tissue plane. Hence, four material parameters and a global fiber orientation were identified (Fig. 12).

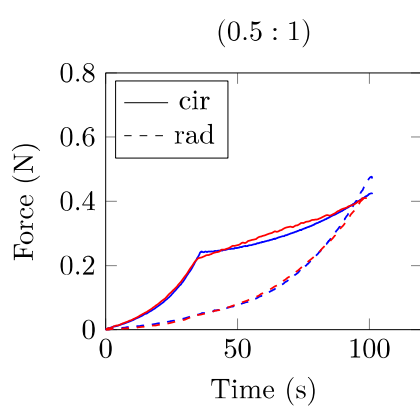
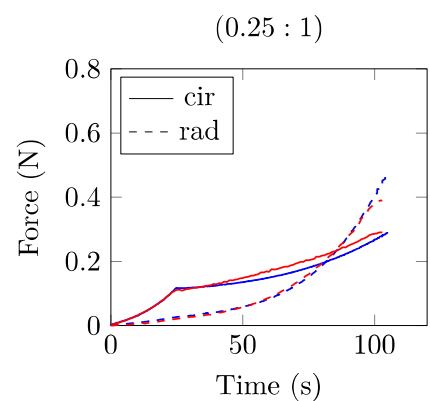
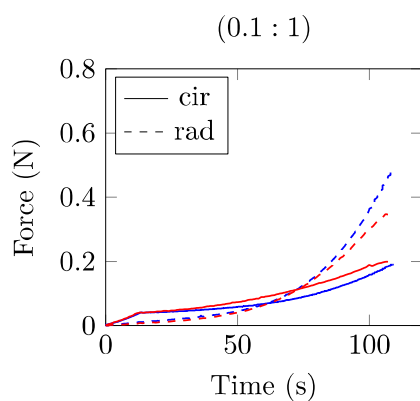
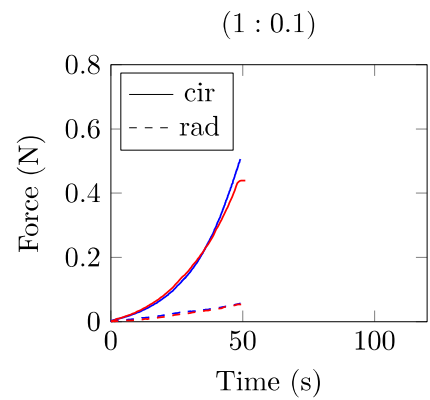
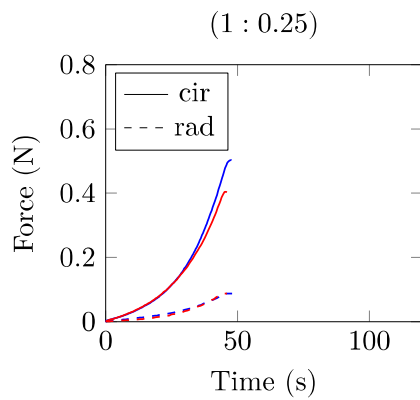
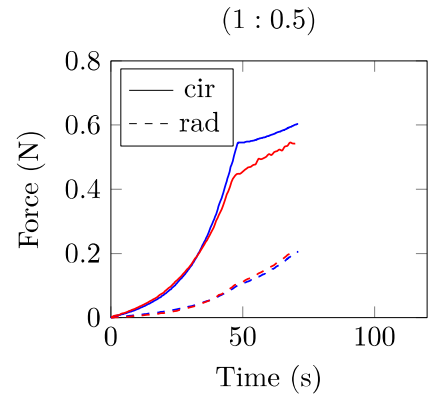
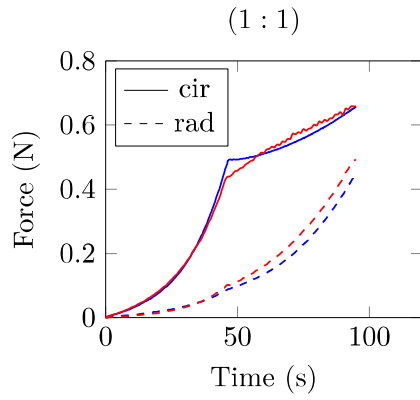


Fig. 12: Forces in radial and circumferential directions from experimental (blue) and inverse analysis (red) results. A unique and global orientation angle was identified through inverse analysis, together with the four material parameters

A good agreement between experimental and numerical curves was found.

However, the cost function is still higher than if we consider local fiber orientations. The different sets of parameters obtained, depending on the number of loading conditions used simultaneously, are reported in Table 1.

		Number of loading conditions				
		Fixed $\theta$ (interpolated from confocal measurements)				Free $\theta$
		1	3	5	7	7
Parameters of the modified HGO model	$c_0$	2.5 kPa	6.2 kPa	5.5 kPa	5.9 kPa	4 kPa
	$c_1$	10.3	7.9	8.3	8	9.6
	$c_2$	190 kPa	152 kPa	145.6 kPa	131 kPa	138 kPa
	$c_3$	29.7	33.2	34	34.7	29.4
	$\theta$	-				
Cost function	$\bar{f}$	0.036	0.087	0.07	0.1	0.124

Table 1: Modified HGO model parameters identification depending on the number of experimental loading conditions used

#### 4 DISCUSSION

Thickness measurements should be performed with caution due to the difficulty of obtaining accurate and repeatable thickness values on a very soft tissue with high heterogeneity. Overall, the average thickness is of the same order of magnitude regardless the leaflet, the valve or storage condition of the sample (fresh or frozen).

As the samples are immersed during the tests, 3D-DIC measurements can be affected by optical refraction. Sutton and McFadden (Sutton and McFadden, 1999) have shown that errors are introduced when the angle between the optical axis and the interface changes. But their conclusion was that careful control of the rotation angle between the specimen and the observation system is sufficient to minimize the effect on strain measurements during underwater experiments. Their results also indicate that

the slow fluid motion does not significantly affect strain measurements. Nevertheless, to confirm the accuracy of the measurements despite the isotonic saline bath, a 3-mm rigid body motion of a steel plate was captured using DIC. No significant difference was observed between the displacement values given by the biaxial tensile machine and the DIC system. The noise generated on the picture seems to be negligible.

Like most soft tissues, the structure of AV tissue based on a network of collagen fibers embedded in an elastin matrix is responsible for its anisotropic behavior. The highly non-linear behavior highlighted on stress-strain curves (Fig. 7) is consistent with the literature (Avril and Evans, 2017; Sacks and Sun, 2003). According to Liao et al. (Liao et al., 2007) who studied the relationship between the kinematics of collagen fibrils and the mechanical properties of mitral valve tissues (using Small Angle X-Ray Scattering – SAXS – measurements), the underlying phenomenon of this behavior is mainly due to the increasing number of initially crimped collagen fibers that are recruited during deformation. Collagen fibrils appear to remain in their unstrained configuration until the beginning of the highly non-linear region on the stress-strain curves.

Regarding the different results obtained in terms of radial or circumferential directions, according to Vesely et al. (Vesely, 1998), the elastin fibers of the ventricularis layer, which are mainly oriented in the radial direction, participate equally with collagen during initial circumferential stretching but mainly control the radial behavior, making the tissue response more compliant. This radial extensibility plays an important role during the valve closing stage, in order to avoid retrograde flow thanks to a co-adaptation of the leaflets.

We have seen in section 3.1 that there are no significant differences in the mechanical response at the beginning and at the end of the whole loading protocol. It means that the tissue integrity is preserved, but also that the mechanical behavior is perfectly reproducible, regardless of what the samples has experienced. The mechanical behavior is independent of the material history as long as the damage limit is not reached. Therefore, the scattering of the mechanical response between the different valves cannot be attributed to the deterioration of the sample during the experiments. However, it may be related to tissue variability, and more importantly, to the relative positioning of the sample with the stretching axes. Indeed, small misalignment errors can significantly modify the reorientation of the fibers with respect to the stretching axes.

When one axis stops moving, the displacement of the other axis is responsible for the rotation of the fibers. This rotation of the fibers induces significant realignments and a decrease of strain can occur on the immobile axis. Thus, sometimes, the strain tends to decrease in the circumferential directions when  $T_x$  is very low compared to  $T_y$  (e.g. in the case of (0.1:1) load). This phenomenon is much more visible on fresh samples which means that freezing the valves probably alter the fibrous structure and more specifically the elastin fibers.

For the inverse analysis study, carried out on a perfect monolayer material with a homogeneous thickness, the modified HGO model (with identified parameters) is able to efficiently reproduce most of the experimental observations. Whatever the number of loading conditions used to identify the set of parameters, a good correlation was

obtained between numerical and experimental results. A globally similar quality of results is obtained for all the inverse analysis procedures on their respective loading conditions. However, the identified parameters considerably evolved from the single-load inverse analysis procedure with respect to the seven loading one. An improvement in the predictability of the model was observed while increasing the number of observable elements. A minimum of three different loading conditions seems to be necessary to get an accurate set of parameters that allows to model various loading conditions.

Considering a local or global direction of the fibers did not lead to very different sets of parameters. This is probably due to the fact that in our case the orientation of the fibers is globally homogeneous. Actually, the value of  $\theta$  ( $13.1^\circ$ ) identified at the global level is close to that measured experimentally ( $0 \pm 10^\circ$ ). For more heterogeneous materials in terms of fiber distribution, local information seems necessary.

We limited our study to in vitro experiments. In addition, planar biaxial tensile tests cannot be directly compared to the complex load encountered by the leaflets during cardiac cycles. They only partially reproduce the diastole load, not the systole. **Other kinds of solicitations, more suitable for reproducing representative boundary conditions of the systole, could be used. The bulge inflation tests proposed by Avril to characterize aortic aneurysms could be an option (Avril and Evans, 2017).** The results were obtained in the central region of the leaflet. They could be different in other areas, such as near the commissures where fibers may have a different distribution. The

number of samples tested was also limited. Due to the large spacing between the confocal images relative to the size of the measurement area, the continuity of the local angular information is not ensured. Thus, cubic interpolation on the sample surface may not accurately capture the evolution of angles, especially in the case of discontinuities.

Adding more measurements points could certainly reduce this uncertainty.

## **5 CONCLUSIONS**

A new experimental protocol for the measurement of the mechanical response of porcine AV leaflets is presented in this study. It is based on the combined use of biaxial tensile tests and digital image correlation. Local orientations of the collagen fibers were measured by confocal laser scanning microscopy. Taking this information into account during the identification of material parameters by inverse analysis offer a more relevant set of parameters. Indeed, parameters identified using a global fiber orientation at the same time are less accurate. The modified HGO constitutive model demonstrated its ability to model porcine AV leaflets under a wide range of loading conditions, representative of those encountered during diastole. We have also shown that a single biaxial test, based on a single loading condition, is not sufficient to obtain a relevant set of parameters. The one we obtained using at least three different loading conditions allows us to model a wide range of solicitations. The experimental protocol and the numerical model can now be used to characterize and model natural or artificial materials of the same type. We are confident in the fact that they can now be used to help designers to develop new artificial valves.

## **FUNDING**

This work was supported by CARNOT M.I.N.E.S. [grant 20531]. The authors would like to thank the Mat Xper company for its financial support during the development of the experimental setup.

## REFERENCES

- Amini Khoiy, K., Amini, R., 2016. On the Biaxial Mechanical Response of Porcine Tricuspid Valve Leaflets. *J. Biomech. Eng.* 138, 104504. <https://doi.org/10.1115/1.4034426>
- Avril, S., Evans, S. (Eds.), 2017. *Material Parameter Identification and Inverse Problems in Soft Tissue Biomechanics, CISM International Centre for Mechanical Sciences.* Springer International Publishing, Cham. <https://doi.org/10.1007/978-3-319-45071-1>
- Billiar, K.L., Sacks, M.S., 2000. Biaxial Mechanical Properties of the Natural and Glutaraldehyde Treated Aortic Valve Cusp—Part I: Experimental Results. *J. Biomech. Eng.* 122, 23. <https://doi.org/10.1115/1.429624>
- Buchanan, R.M., Sacks, M.S., 2014. Interlayer micromechanics of the aortic heart valve leaflet. *Biomech. Model. Mechanobiol.* 13, 813–826. <https://doi.org/10.1007/s10237-013-0536-6>
- Candau, N., Pradille, C., Bouvard, J.-L., Billon, N., 2016. On the use of a four-camera stereovision system to characterize large 3D deformation in elastomers. *Polym. Test.* 56, 314–320. <https://doi.org/10.1016/j.polymertesting.2016.10.017>
- Eckert, C.E., Fan, R., Mikulis, B., Barron, M., Carruthers, C.A., Friebe, V.M., Vyavahare, N.R., Sacks, M.S., 2013. On the biomechanical role of glycosaminoglycans in the aortic heart valve leaflet. *Acta Biomater.* 9, 4653–4660. <https://doi.org/10.1016/j.actbio.2012.09.031>
- Fehervary, H., Smoljkić, M., Vander Sloten, J., Famaey, N., 2016. Planar biaxial testing of soft biological tissue using rakes: A critical analysis of protocol and fitting process. *J. Mech. Behav. Biomed. Mater.* 61, 135–151. <https://doi.org/10.1016/j.jmbbm.2016.01.011>
- Ferreira, T., Rasband, W., 2012. ImageJ User Guide—IJ 1.46r.
- Gasser, T.C., Ogden, R.W., Holzapfel, G.A., 2006. Hyperelastic modelling of arterial layers with distributed collagen fibre orientations. *J. R. Soc. Interface* 3, 15–35. <https://doi.org/10.1098/rsif.2005.0073>
- Genovese, K., Lee, Y.U., Humphrey, J.D., 2011. Novel optical system for *in vitro* quantification of full surface strain fields in small arteries: II. Correction for refraction and illustrative results. *Comput. Methods Biomech. Biomed. Engin.* 14, 227–237. <https://doi.org/10.1080/10255842.2010.545824>
- Ghanbari, H., Viatge, H., Kidane, A.G., Burriesci, G., Tavakoli, M., Seifalian, A.M., 2009. Polymeric heart valves: new materials, emerging hopes. *Trends Biotechnol.* 27, 359–367. <https://doi.org/10.1016/j.tibtech.2009.03.002>
- Holzapfel, G.A., Gasser, T., Ogden, R.W., 2000. A New Constitutive Framework for Arterial Wall Mechanics and a Comparative Study of Material Models. *J. Elast. Phys. Sci. Solids* 61, 1–48. <https://doi.org/10.1023/A:1010835316564>
- Kidane, A.G., Burriesci, G., Edirisinghe, M., Ghanbari, H., Bonhoeffer, P., Seifalian, A.M., 2009. A novel nanocomposite polymer for development of synthetic heart valve leaflets. *Acta Biomater.* 5, 2409–2417. <https://doi.org/10.1016/j.actbio.2009.02.025>
- Lee, T.C., Midura, R.J., Hascall, V.C., Vesely, I., 2001. The effect of elastin damage on the mechanics of the aortic valve. *J. Biomech.* 34, 203–210.

- Liao, J., Yang, L., Grashow, J., Sacks, M.S., 2007. The Relation Between Collagen Fibril Kinematics and Mechanical Properties in the Mitral Valve Anterior Leaflet. *J. Biomech. Eng.* 129, 78. <https://doi.org/10.1115/1.2401186>
- Mohammadi, H., Mequanint, K., 2011. Prosthetic aortic heart valves: Modeling and design. *Med. Eng. Phys.* 33, 131–147. <https://doi.org/10.1016/j.medengphy.2010.09.017>
- Mozaffarian, D., Benjamin, E.J., Go, A.S., Arnett, D.K., Blaha, M.J., Cushman, M., Das, S.R., de Ferranti, S., Després, J.-P., Fullerton, H.J., Howard, V.J., Huffman, M.D., Isasi, C.R., Jiménez, M.C., Judd, S.E., Kissela, B.M., Lichtman, J.H., Lisabeth, L.D., Liu, S., Mackey, R.H., Magid, D.J., McGuire, D.K., Mohler, E.R., Moy, C.S., Muntner, P., Mussolino, M.E., Nasir, K., Neumar, R.W., Nichol, G., Palaniappan, L., Pandey, D.K., Reeves, M.J., Rodriguez, C.J., Rosamond, W., Sorlie, P.D., Stein, J., Towfighi, A., Turan, T.N., Virani, S.S., Woo, D., Yeh, R.W., Turner, M.B., 2016. Heart Disease and Stroke Statistics—2016 Update: A Report From the American Heart Association. *Circulation* 133, e38–e360. <https://doi.org/10.1161/CIR.0000000000000350>
- Roux, E., 2011. Assemblage mécanique : stratégies d’optimisation des procédés et d’identification des comportements mécaniques des matériaux (Thèse). École Nationale Supérieure des Mines de Paris, École Nationale Supérieure des Mines de Paris.
- Roux, E., Bouchard, P.-O., 2015. On the interest of using full field measurements in ductile damage model calibration. *Int. J. Solids Struct.* 72, 50–62. <https://doi.org/10.1016/j.ijsolstr.2015.07.011>
- Roux, E., Bouchard, P.-O., 2013. Kriging metamodel global optimization of clinching joining processes accounting for ductile damage. *J. Mater. Process. Technol.* 213, 1038–1047. <https://doi.org/10.1016/j.jmatprotec.2013.01.018>
- Sacks, M.S., 2000. Biaxial Mechanical Evaluation of Planar Biological Materials. *J. Elast. Phys. Sci. Solids* 61, 199. <https://doi.org/10.1023/A:1010917028671>
- Sacks, M.S., David Merryman, W., Schmidt, D.E., 2009. On the biomechanics of heart valve function. *J. Biomech.* 42, 1804–1824. <https://doi.org/10.1016/j.jbiomech.2009.05.015>
- Sacks, M.S., Sun, W., 2003. Multiaxial Mechanical Behavior of Biological Materials. *Annu. Rev. Biomed. Eng.* 5, 251–284. <https://doi.org/10.1146/annurev.bioeng.5.011303.120714>
- Schenke-Layland, K., 2008. Non-invasive multiphoton imaging of extracellular matrix structures. *J. Biophotonics* 1, 451–462. <https://doi.org/10.1002/jbio.200810045>
- Stella, J.A., Liao, J., Sacks, M.S., 2007. Time-dependent biaxial mechanical behavior of the aortic heart valve leaflet. *J. Biomech.* 40, 3169–3177. <https://doi.org/10.1016/j.jbiomech.2007.04.001>
- Stella, J.A., Sacks, M.S., 2007. On the Biaxial Mechanical Properties of the Layers of the Aortic Valve Leaflet. *J. Biomech. Eng.* 129, 757. <https://doi.org/10.1115/1.2768111>
- Sutton, M.A., McFadden, C., 1999. Development of a methodology for non-contacting strain measurements in fluid environments using computer vision. *Opt. Lasers Eng.* 32, 367–377. [https://doi.org/10.1016/S0143-8166\(99\)00066-4](https://doi.org/10.1016/S0143-8166(99)00066-4)

- Sutton, M.A., Yan, J.H., Tiwari, V., Schreier, H.W., Orteu, J.J., 2008. The effect of out-of-plane motion on 2D and 3D digital image correlation measurements. *Opt. Lasers Eng.* 46, 746–757. <https://doi.org/10.1016/j.optlaseng.2008.05.005>
- Vesely, I., 1998. The role of elastin in aortic valve mechanics. *J. Biomech.* 31, 115–123.
- Wang, H.M., Luo, X.Y., Gao, H., Ogden, R.W., Griffith, B.E., Berry, C., Wang, T.J., 2014. A modified Holzapfel-Ogden law for a residually stressed finite strain model of the human left ventricle in diastole. *Biomech. Model. Mechanobiol.* 13, 99–113. <https://doi.org/10.1007/s10237-013-0488-x>

## FIGURE CAPTIONS LIST

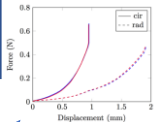
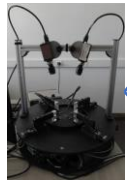
- Fig. 1 Custom biaxial tensile device
- Fig. 2 Dissected porcine AV leaflet: square-shaped sample with gripping device and speckle pattern (subset grid size of 29 px)
- Fig. 3 Specimen examined under the confocal laser scanning microscope
- Fig. 4 Averaged thickness of the samples with dispersion for each valve
- Fig. 5 (1:1) curves obtained at the beginning and at the end of a full loading protocol, on the same sample
- Fig. 6 Strain and norm of displacement fields obtained on frozen (left) and fresh (right) samples
- Fig. 7 Example of tension-strain curves for the (1:1) loading condition for several frozen and fresh samples
- Fig. 8 Four pictures of collagen fibers from a total stack of 140  $\mu\text{m}$  depth
- Fig. 9 Interpolated angles ( $^{\circ}$ ) on a real scale grid (mm) for the mechanically tested sample
- Fig. 10 Interpolation of measured fibers directions on the undeformed finite element mesh
- Fig. 11 Forces in radial and circumferential directions from experimental (blue) and inverse analysis (red) results. Local fiber orientation, measured with confocal microscopy, was fixed and interpolated on each element

**Fig. 12** Forces in radial and circumferential directions from experimental (blue) and inverse analysis (red) results. A unique and global orientation angle was identified through inverse analysis, together with the four material parameters

## TABLE CAPTION LIST

Table 1 Modified HGO model parameters identification depending on the number of experimental loading conditions used

Biaxial  
tensile test  
+ DIC

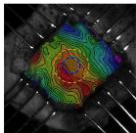


Force vs  
displacement

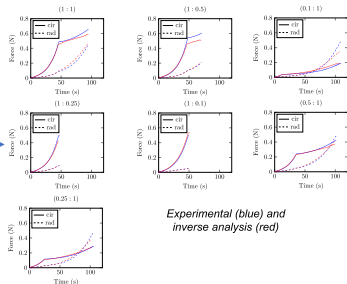
Finite element model  
with *modified HGO*  
constitutive equation

$$W = \frac{c_0}{c_1} [e^{c_1(\bar{I}_1 - 3)} - 1] + \frac{c_2}{2c_3} [e^{c_3(\kappa\bar{I}_1 + (1-3\kappa)\bar{I}_4 - 1)^2} - 1]$$

Strain fields

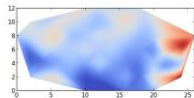
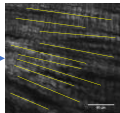


Parameters'  
identification  
(inverse  
analysis)



Experimental (blue) and  
inverse analysis (red)

Confocal  
microscopy



Collagen fibers'  
orientation

Good agreement between  
experimental and numerical force-  
displacement curves for several  
loading conditions